phys. stat. sol. (a) **205**, No. 3, 633–646 (2008) / **DOI** 10.1002/pssa.200723410

physica status solidi a
www.pss-a.com
applications and materials science

Feature Article

Carbon nanotube transistors – chemical functionalization and device characterization

Kannan Balasubramanian[1], Eduardo J. H. Lee[1], Ralf Thomas Weitz[1], Marko Burghard[*,1], and Klaus Kern[1,2]

[1] Max-Planck-Institut für Festkörperforschung, Heisenbergstraße 1, 70569 Stuttgart, Germany
[2] Institut de Physique des Nanostructures, École Polytechnique Fédérale de Lausanne, 1015 Lausanne, Switzerland

Received 1 September 2007, accepted 30 November 2007
Published online 25 February 2008

PACS 61.46.Fg, 73.30.+y, 82.45.Yz, 85.30.Tv, 85.35.Kt

[*] Corresponding author: e-mail m.burghard@fkf.mpg.de, Phone: +49 711 689 1448, Fax: +49 711 689 1662

This review presents an overview of the recent progress made in the field of carbon nanotube (CNT)-based field-effect transistors (FETs). Starting from the simplest device architectures, various methods reported for fabricating CNT-FETs are presented. The main focus is laid on the use of chemical functionalization strategies both at a tube and at a device level to improve the performance of the devices. In addition to solid dielectric gate insulators, the use of liquids or solid polymer electrolytes as effective electrochemical gating media is outlined. Following this, device parameters of the various CNT-FETs are compared and discussed. Finally, the utility of scanning photocurrent microscopy as an efficient characterization tool to estimate electronic band-profiles of CNT-FETs is highlighted. The review concludes with future perspectives in this rapidly emerging field.

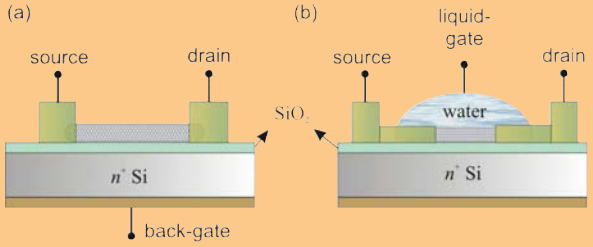

The figure displays schematics of (a) a back-gated and (b) an electrochemically-gated FET incorporating an individual semiconducting single-wall carbon nanotube as the channel.

1 Introduction Carbon Nanotubes (CNTs) are emerging as promising components of molecular-scale electronic devices [1], due to their excellent electrical properties including large current densities of $\geq 10^9$ A/cm^2 [2] and field-effect mobilities that considerably exceed the intrinsic mobility of silicon [3]. Basic components of electronic circuits such as field-effect transistors (FETs) [4], logic gates [5] and memory elements [6] have been demonstrated based on CNTs. Despite these impressive advancements, a number of factors have been hampering the widespread application of CNTs in the semiconductor industry. The major task of the present review is to demonstrate that chemical functionalization represents a highly versatile strategy to overcome several of these hurdles. When applied to appropriate device architectures, the functionalization approach yields CNT-FETs whose performance successfully rivals that of state-of-the-art metal-oxide-semiconductor FETs (MOSFETs).

The paper is organized as follows. After the introduction, a brief overview of the fundamentals of CNTs and CNT-based FETs will be given. The next section describes a range of chemical functionalization schemes that have been devised for the performance enhancement of CNT-FETs. The subsequent section is devoted to the characterization of as-prepared and functionalized CNT-FETs through electrical transport measurements and scanning photocurrent microscopy. In this context, the relevant device parameters of the FETs such as saturation behavior, field-effect mobility, transconductance and sub-threshold slope will be analyzed and compared. The review con-

cludes with future perspectives for the fabrication of CNT-based FETs.

2 Carbon nanotubes – fundamentals

2.1 Physical and electronic structure Carbon nanotubes can be visualized as concentric cylinders of graphene sheets, which are single atomic layers of graphite. They are classified as single-wall (SWCNTs) comprised of just a single shell, and multi-wall (MWCNTs) comprised of at least two shells of the graphene sheet. The scope of this review is restricted to SWCNTs. Based on its orientation with respect to the hexagonal graphene lattice, the structure of a nanotube can be completely specified through the chiral vector $\boldsymbol{C}_h$ given by $\boldsymbol{C}_h = n\boldsymbol{a}_1 + m\boldsymbol{a}_2$ (n, m are integers), denoted as (n,m), where $\boldsymbol{a}_1$ and $\boldsymbol{a}_2$ are the real space unit vectors of the hexagonal lattice of graphene (see Fig. 1).

SWCNTs can be produced by a variety of methods, namely arc-discharge [7], laser ablation [8], high pressure pyrolysis of carbon monoxide (HiPco [9]) and chemical vapor deposition [10, 11]. All of these methods combine a carbon source such as graphite, carbon monoxide, ethanol or methane with a catalyst in the form of metal particles [12]. The commonly investigated HiPco SWCNTs exhibit a relatively broad diameter distribution of 0.7–1.1 nm [9]. By controlling the size distribution of the catalyst particles, it is possible to restrict the diameter range of the synthesized nanotubes [13]. It is an intriguing property of CNTs that their electronic structure varies drastically even within a small diameter range. In a first approximation, it can be derived from that of graphene by applying the zone-folding approach [14]. Figure 2 displays the calculated electronic structure of a (9,0) and a (10,0) tube. Although the diameters of the two tubes differ by just one Ångstrom, the (9,0) tube is metallic while the (10,0) tube is semiconducting. As a general rule, (n,m) tubes with ($n - m$) being an integer multiple of 3 are metallic (m-SWCNTs), while the remaining tubes are semiconducting (s-SWCNTs). The band-gap of the s-SWCNTs can be approximated by the relation

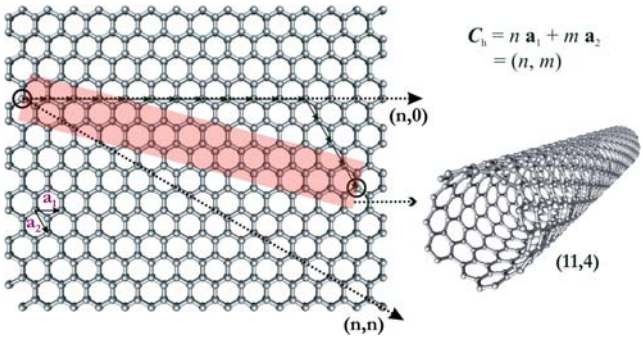

Figure 1 (online colour at: www.pss-a.com) Physical structure of a carbon nanotube starting from a graphene sheet, whose unit vectors $\boldsymbol{a}_1$ and $\boldsymbol{a}_2$ are shown. Every nanotube is uniquely determined by its chiral vector $\boldsymbol{C}_h = (n,m)$. The (11,4) nanotube is obtained by rolling the graphene sheet along the red shaded region.

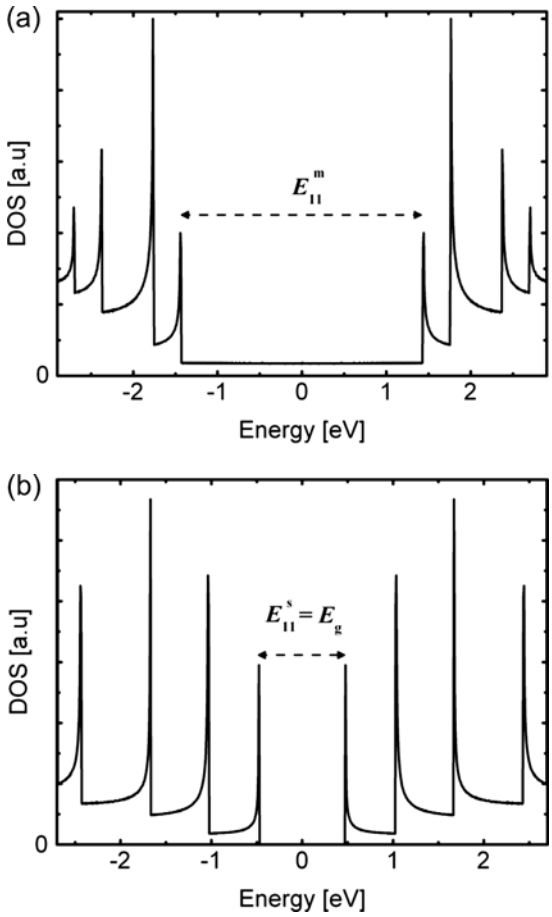

Figure 2 Calculated electronic density of states (DOS) of (a) the (9,0) and (b) the (10,0) tube as obtained from tight-binding calculations with the overlap energy $\gamma_0 = -2.7$ eV. While the (9,0) having a finite density of states at the Fermi level is metallic, the (10,0) tube is semiconducting.

$E_g = 0.8$ eV/d, where d is the diameter of the nanotube in nm [15].

2.2 Field-effect transistors based on single SWCNTs The prediction that SWCNTs can be semiconducting motivated the fabrication of FETs containing individual SWCNTs as conducting channel. The first devices [4, 16] as well as most of the SWCNT-FETs realized so far are fabricated in a back-gate configuration. In such devices, a single semiconducting SWCNT is contacted by metal electrodes defined by e-beam lithography (see Fig. 3), with the standard substrate being silicon covered by a thermally grown oxide of thickness in the range of 100 nm to 1 μm that serves as the gate insulator. Unlike a conventional MOSFET, the SWCNT-FET functions like a Schottky-Barrier FET (SBFET) [17]. Moreover, compared to the former type of device, it is more difficult to implement ohmic contacts in a SWCNT-FET, since most electrode metals lead to Schottky barrier formation at the contacts to the nanotube, due to mismatch in the work functions of the two materials and the formation of metal–carbon bonds

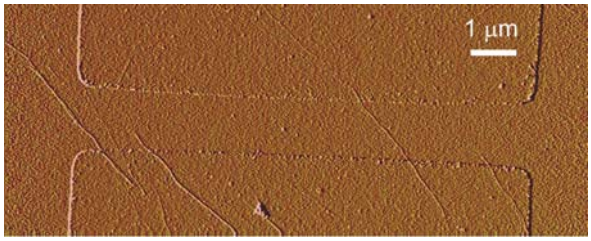

Figure 3 (online colour at: www.pss-a.com) An atomic force microscope (AFM) amplitude image of a field-effect transistor comprising of a single semiconducting carbon nanotube contacted with electrodes separated by ~1.5 μm.

[18]. As depicted in Fig. 4(a), this barrier is pinned such that a variation in the gate potential merely shifts the nanotube sub-bands [19, 20]. Carrier injection thus takes place through thermionic emission and tunneling across the Schottky barriers, whose width depends on the applied gate voltage [21]. Figure 4(b) compares the dependence of conductance for a contacted m- and s-SWCNT as a function of back-gate voltage. While the conductance of the m-SWCNT remains fairly constant over the entire gate voltage range, the s-SWCNT conductance can be modulated over more than three orders of magnitude.

The first SWCNT-FETs exhibited high resistances and poor switching characteristics [4, 16]. The height of the Schottky barriers, which limits the ON conductance of these devices, depends on the type of metal used for contacting the tubes. Improved device performance has been achieved with two different contact metals. In the first case, Ti is used as the metal and the device is annealed under Argon at a temperature of 800 °C [22], whereupon TiC is formed at the contacts which facilitates carrier injection (both electrons and holes) leading to high ON currents. Alternatively, the use of Pd as contact metal directly yields devices displaying near-to-ballistic ON conductance [23]. The reason why especially Pd makes particularly good contacts with s-SWCNTs is not yet fully understood, although it appears that the extraordinary wetting properties of Pd play an important role [23]. However, it is important to keep in mind that even with Pd contacts, due to the large variation in the band-gap of the semiconducting tubes, the fabricated devices exhibit a broad distribution of ON conductances (up to an order of magnitude).

Unless subjected to further treatment, SWCNT-FETs in general show p-type characteristics (Fig. 4(b)), which has been attributed to oxygen adsorption causing p-type doping of the nanotube and/or a change in the work function of the metal contact [24, 25]. It is worthy to note that for larger diameter s-SWCNTs, as a consequence of their small band-gap, the barrier heights are greatly reduced for both electrons and holes [26]. The corresponding FETs exhibit ambipolar characteristics, as exemplified in Fig. 4(c) for an FET comprising a nanotube with a diameter of ~2 nm. Ambipolar SWCNT-FETs are promising for the implementation of novel device architectures such as XOR gates with a minimal device count of just one [27]. Figure 4(b) furthermore reveals that the transfer characteristics measured under ambient conditions are usually imprinted with a pronounced hysteresis. The origin of this hysteresis has been ascribed to charge traps in the vicinity of the nanotube, which may be related to surface-bound water

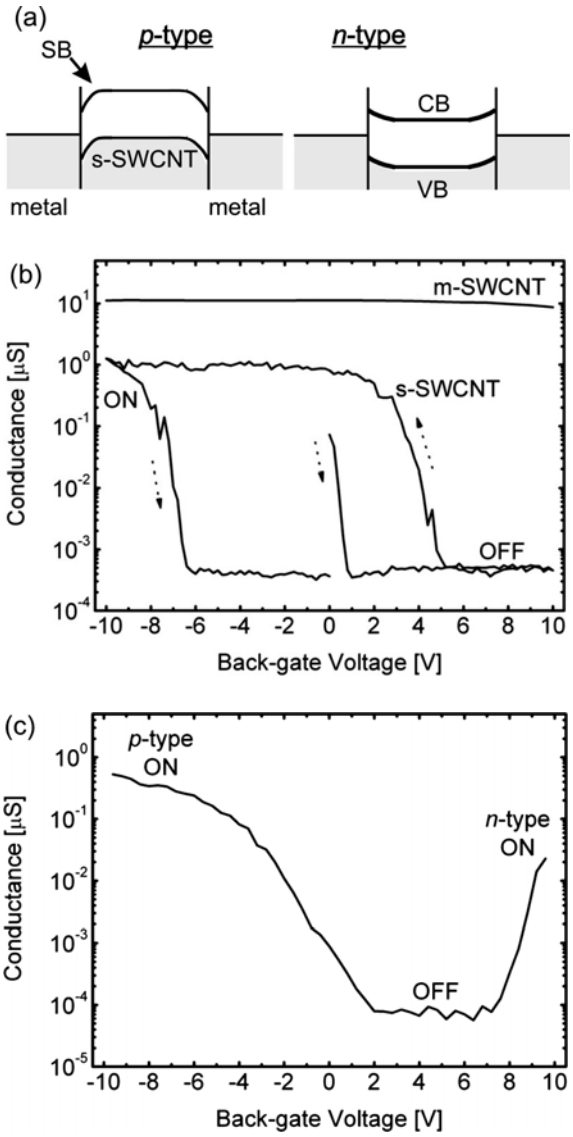

Figure 4 (a) Simplified view of the electronic band structure of a field-effect transistor made of a single semiconducting nanotube (s-SWCNT) as the channel. At negative back-gate voltages, the bands are bent upwards and injection of holes is favored, while at positive back-gate voltages, electron injection is favored. (b) Variation of conductance of an m-SWCNT and an s-SWCNT as a function of the gate voltage. While the m-SWCNT conductance remains unaltered over the entire gate voltage range, the conductance of the s-SWCNT can be modulated by at least 3 orders of magnitude. (c) Back-gate dependence of conductance for a large diameter (2 nm) s-SWCNT showing ambipolar behaviour. Drain–source bias (V_{ds}) for the m-SWCNT and s-SWCNTs is 1 mV and 100 mV, respectively.

molecules on the SiO_2 or water molecules trapped inside the oxide layer [28].

2.3 CNT-FETs based on electrochemical field-effect An alternative design for CNT-FETs involves the use of a liquid electrolyte as gating medium. While this approach does not appear promising for semiconductor electronics, it offers a number of other advantages including a highly efficient gate coupling (see Section 2.4), as well as the possibility of fabricating FET-based nanoscale sensors in liquids [29]. An electric field-effect inside an aqueous electrolyte was first observed using a MWCNT [30], and later also for SWCNTs [31]. In the latter experiments, devices with individual s-SWCNTs were immersed in an aqueous electrolyte solution, and a standard reference electrode (e.g., Ag/AgCl) used as the gate electrode. Due to the ionic conductivity of the medium, application of a gate voltage leads to the formation of an electrochemical double layer (Helmholtz layer) at the nanotube-electrolyte interface [32]. Variation of the gate voltage leads to charging and discharging of this layer, which shifts the Fermi level of the contacted nanotube and thereby modulates its conductance. We have observed that even in the absence of an electrolyte gate switching can be achieved, as demonstrated by Fig. 5 for a single s-SWCNT immersed in distilled water. It furthermore turned out that the key factor determining whether a solvent works as an effective gating medium is a certain polarizability, as is the case for water, ethanol, *N*-methyl formamide and *N*,*N*-dimethylformamide. Alternative gating media for the fabrication of electrochemical SWCNT-FETs are solid polymer electrolytes (SPE) [33, 34] or ionic liquids [35].

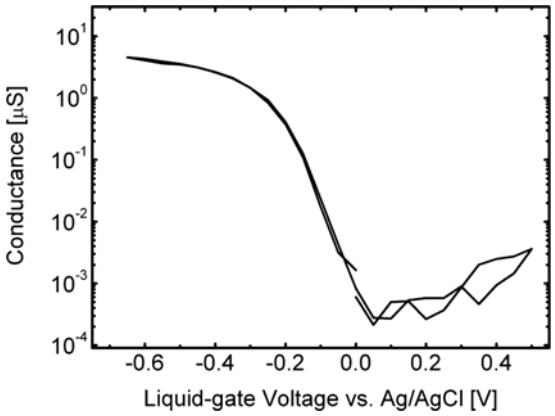

Figure 5 Variation of conductance of an individual s-SWCNT as a function of the liquid gate voltage ($V_{ds} = \pm 10$ mV). A water droplet placed on the contacted tube serves as the gating medium with a thin Ag/AgCl wire functioning as the gate electrode. Hysteresis-free field-effect behaviour is clearly observed in a very small gate voltage range. The water droplet (resistivity: 18.2 MΩ cm) was protected with a thin layer of non-volatile solvent (squalane) to avoid evaporation and to maintain its resistivity.

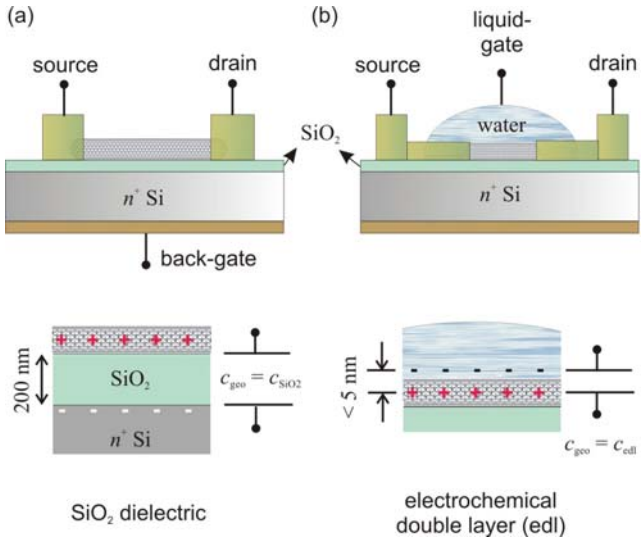

Figure 6 (online colour at: www.pss-a.com) Model of geometric gate capacitances for (a) back-gated and (b) electrochemically gated SWCNT-FETs. In the case of back-gating, the geometric capacitance is determined by the capacitance of the SiO_2 dielectric. During electrochemical gating the electrochemical double layer (edl) formed at the interface between the tube and the liquid determines the geometric capacitance. The thickness of the edl is determined by the Debye length which is in turn a function of the electrolyte concentration.

2.4 Role of capacitances The strength of the gating effect in CNT-FETs is governed by the capacitance occurring between the gate electrode and the nanotube channel [31]. As a basis for the discussions presented in the next sections, we first describe capacitance models for the two gating configurations described above. In the case of Schottky barrier CNT-FETs based on dielectric gate insulators, the gate electrode has to be positioned above or below the source and drain contacts, in order to be able to tune the transmission through the barriers. The gating effect here is thus determined by the dielectric capacitance of the insulating layer between the nanotube and the gate electrode, as shown in Fig. 6(a). This capacitance can be best modeled by assuming cylindrical capacitor geometry [36]. The capacitance per unit tube length is then given by $c_{ox} = 2\pi\varepsilon_r\varepsilon_0/\ln(2(t_{ox} + r)/r)$, where ε_r is the dielectric constant of the oxide layer (~4 for SiO_2), ε_0 is the vacuum permittivity, t_{ox} is the thickness of the oxide layer, and r is the radius of the nanotube. Assuming an oxide thickness of 100 nm and a nanotube radius of 1 nm, a value of ~37 pF/m is obtained for c_{ox}. Importantly, due to the lower density of electronic states in the quasi-1D nanotubes in comparison to bulk semiconductors, the so-called quantum capacitance has to be taken into account as a second contribution in series with the geometric oxide capacitance [31]. The quantum capacitance per unit tube length can be calculated as $c_q = e^2 g(E)$, where $g(E)$ is the electronic density of states which can be approximated to 400 pF/m [31]. The lower of the two capacitances dominates the total ca-

pacitance. Accordingly, the net capacitance for the above back-gated s-SWCNT-FET is given by $c_{\text{bg-single}} = (c_{\text{ox}}^{-1} + c_{\text{q}}^{-1})^{-1} = 34$ pF/m, very close to the value of the geometric capacitance.

Enhancement of the coupling efficiency requires increasing the gate capacitance, which can be attained either by increasing ε_{r} (high-κ dielectrics) or by reducing the thickness of the gate oxide. Both strategies have been realized in back- [37] and top- [38] gate geometry. For instance, an 8 nm thick ZrO_2 ($\varepsilon_{\text{r}} = 25$) layer has been used as top gate insulator, which yields a geometric capacitance of 550 pF/m [38]. In this case, the net capacitance is 230 pF/m, which is one order of magnitude larger than for the corresponding back-gated FET with a SiO_2 insulator of 100 nm thickness. However, the net capacitance at the same time determines the field-effect mobility of the device [36]. Since a decreased capacitance leads to increased mobility, there is a trade-off between improved gate coupling and higher field-effect mobility. It should furthermore be noted that although the gate voltage range is appreciably reduced in local top-gate devices, their operation still requires permanent application of a constant back-gate voltage. An alternative approach utilizes aluminium electrodes as back-gate, whose insulating native oxide layer (~few nm thickness) ensures low operating voltages [5].

The scenario for a CNT-FET immersed in a liquid or coated with an SPE is illustrated in Fig. 6(b), which reveals that the geometric capacitance is determined by the Debye length (λ_{D}) of the Helmholtz layer. A simple estimate for this double-layer capacitance is given by $c_{\text{edl}} = 2\pi\varepsilon_{\text{r}}\varepsilon_0 / \ln(1 + \lambda_{\text{D}}/r)$ [31]. For water ($\varepsilon_{\text{r}} = 80$) and a low concentration of ions ($\lambda_{\text{D}} \sim 4$ nm to 5 nm) [39], c_{edl} is of the order of 2000 pF/m. Like for the back gate configuration, this capacitance occurs in series with the quantum capacitance, yielding a net capacitance of around 330 pF/m, very close to the theoretical limit of 400 pF/m. It thus becomes evident that the performance of liquid-gated transistors surpasses transistors comprising solid dielectric gate insulators. By increasing the electrolyte concentration and thereby reducing the Debye length, the net capacitance for the liquid-gated configuration can be increased further. Moreover, in contrast to back-gated CNT-FETs, liquid-gated CNT-FETs are independent of device geometry, since in the latter devices the quantum capacitance is dominating. However, in both gate configurations, the maximum capacitance limit is set by the quantum limit of 400 pF/m.

3 Chemical functionalization

3.1 Motivation and strategies In the last section, different fabrication approaches to CNT-FETs have been presented, along with device engineering strategies to improve the performance of the devices. Chemical functionalization methodologies such as doping or the realization of electrochemical FETs, offer an effective means for enhancing the device performance further. As a spin-off, (bio-)chemical sensors based upon FET operation become accessible, wherein functional groups are attached to the nanotubes in order to obtain specificity toward analytes [40, 41]. In this section, we demonstrate how simple chemical modification methods allow mitigating a number of problems inherent to back-gated CNT-FETs, as well as obtaining all-semiconducting nanotube ensembles suitable as FET channels.

Chemical functionalization approaches for CNT-based devices can be classified into two categories, namely modification involving the whole device, and functionalization of only the nanotube channel. For whole device modification, the FET is either immersed in a solvent containing the desired reagent, or the reagent is spin-coated or spotted from the solvent. Nanotube functionalization, on the other hand, can be performed in three different ways, i.e., thermally-activated chemistry, photochemistry, and electrochemistry [42]. Among those, electrochemistry is emerging to be the most controllable and versatile method for obtaining functionalized nanotube devices. In the following subsections, first whole device modification will be discussed, followed by controlled electrochemical functionalization of nanotubes and chemical doping. Finally, a brief description of chemical sensors based on functionalized CNT-FETs is given.

3.2 Chemically modified devices An important requirement for efficient FET device operation is the absence of hysteresis. As mentioned above, hysteresis arises mainly due to the presence of traps in the vicinity of the nanotube. It can be eliminated by reducing the trap/surface defect density, as has been demonstrated through incorporation of a high-quality hydrophobic organic layer between nanotube and the SiO_2. For this purpose, the Si/SiO_2 ($t_{SiO_2} = 4$ nm) substrates have been covered by a self-assembled monolayer (SAM) prepared from 18-phenoxy-octadecyltrichlorosilane [43], as shown in Fig. 7(a). The resulting SWCNT-FETs display an unprecedented combination of device parameters, most notably a very low operating voltage (~1V), an excellent $I_{\text{ON}}/I_{\text{OFF}}$ ratio ($>10^5$), and a very low subthreshold swing of 60 mV/dec at room temperature as is apparent from Fig. 7(b). An alternative strategy is to coat the FETs with appropriate polymers such as polyethyleneoxide (PEO) that can neutralize the trap states due to their donor capability. One example of hysteresis reduction realized in this manner is provided by Fig. 8.

Upon addition of lithium perchlorate ($LiClO_4$) to the PEO matrix, SWCNT-FETs with a solid polymer electrolyte (SPE) coating are obtained [33, 34]. In addition to hysteresis elimination, this imparts the possibility to electrochemically gate the FET. To this end, a micro-fabricated gold electrode on the surface of the substrate or an Ag/AgCl wire in contact with the polymer coating is used as the gate electrode. The resulting SWCNT-FETs can be operated within a gate voltage range that is approximately ten times smaller than for corresponding devices in back gate configuration (100 nm SiO_2 thickness). By variation of the SPE composition, it is possible to tune the threshold

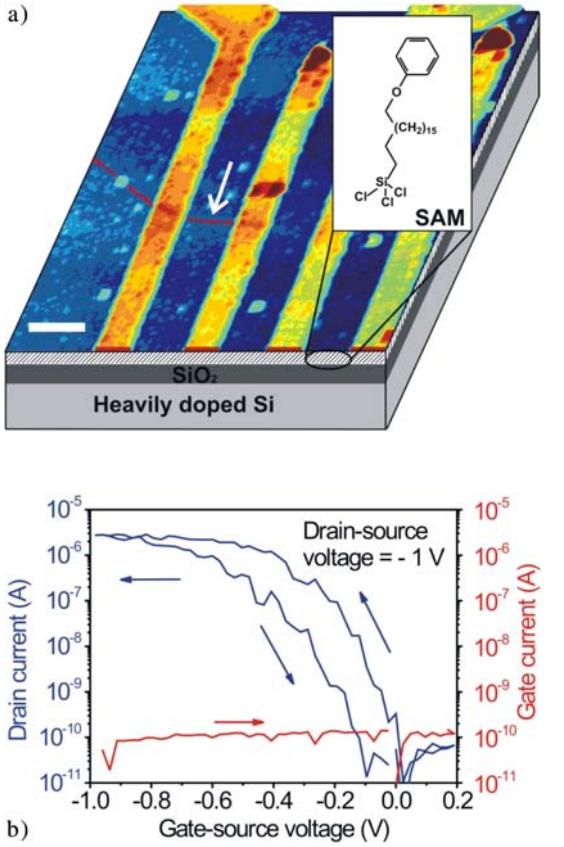

Figure 7 (online colour at: www.pss-a.com) (a) Schematic depiction of an s-SWCNT-FET, with the gate insulator comprising of an organic self-assembled monolayer (SAM) made of (18-phenoxyoctadecyl)trichlorosilane. (b) Gate-dependence of the fabricated device as a function of the back-gate voltage showing low-hysteresis, high sub-threshold swing and low operating voltages. (Reprinted with permission from [43].)

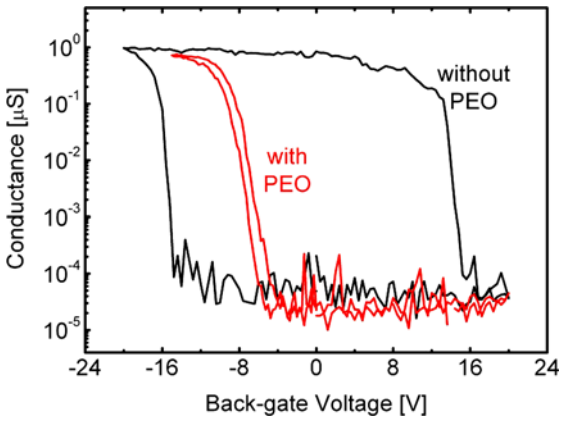

Figure 8 (online colour at: www.pss-a.com) Removal of hysteresis through chemical modification demonstrated by the back-gate dependence of conductance of a single s-SWCNT FET (V_{ds} = 100 mV). A drop of 1 mg/ml of polyethyleneoxide (PEO) in acetonitrile was spotted on the substrate and let to dry.

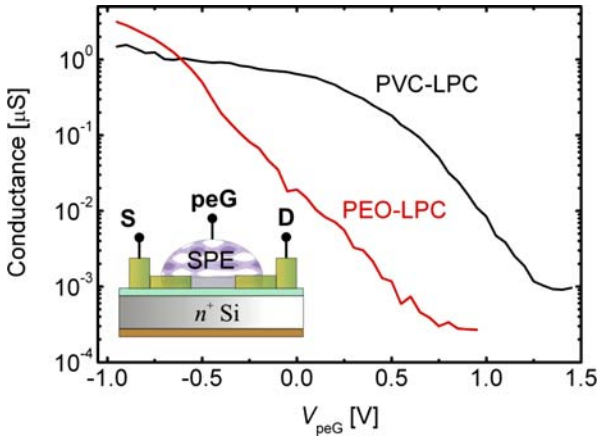

Figure 9 (online colour at: www.pss-a.com) Electrochemical gating of SWCNT-FETs covered with two different solid polymer electrolytes (SPEs). The SPEs were spotted from solution on top of the FET surface and heated at 60 °C for an hour. Conductance of the same individual s-SWCNT (V_{ds} = ±0.1 V) with two different SPEs is plotted as a function of the voltage at the polymer-electrolyte-gate (V_{peG}). An adjacent microfabricated AuPd electrode (~200 μm distance) on the substrate was used as the gate electrode. PEO-LPC: 20 mg/ml polyethyleneoxide, 10 mg/ml lithium perchlorate in a mixture of methanol/water (v/v 4:1). PVC-LPC: 20 mg/ml polyvinylchloride, 2 mg/ml lithium perchlorate in tetrahydrofuran. It is apparent that by changing the composition of the polymer matrix, it is possible to shift the threshold voltage of the transistors. The inset shows the schematic of the fabricated FET (S – source, D – drain).

voltage of the obtained transistors, and thus to fabricate either depletion- or enhancement-mode transistors. An example is the replacement of PEO by polyvinylchloride (PVC) [44, 45], whereby the threshold voltage is shifted to more positive voltages (see Fig. 9). The SPE-coated FETs were found to be stable under ambient conditions for up to four weeks.

3.3 Electrochemical functionalization As mentioned before, electrochemical functionalization (ECM) is a suitable means to alter mainly the contacted tube regions of the FET [46]. ECM is performed either potentiostatically (at constant potentials) or galvanostatically (at constant currents) in a solution containing a reagent as precursor for a reactive chemical species (e.g., a radical) that will be formed via electron transfer with the nanotube [47]. The precursor is usually an organic molecule comprising a reactive end-group and a persistent functional group that the nanotube surface would possess after the modification. Since many organic radical species have a tendency to react with the precursor or to self-polymerize, a polymer coating is often formed on the tubes.

Toward the coupling of organic moieties onto nanotubes, we have devised two schemes that enable grafting a variety of functional groups either covalently or non-cova-

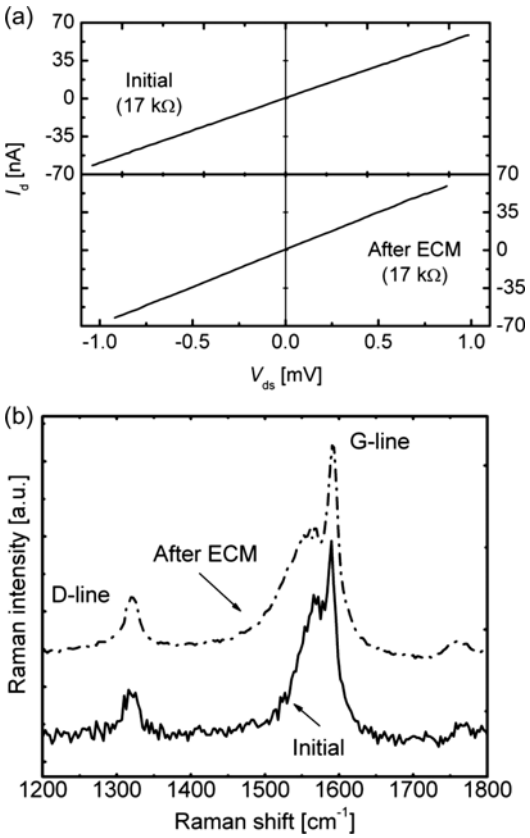

Figure 10 Oxidative electrochemical modification (oECM) of individual contacted m-SWCNTs using a substituted aromatic amine. (a) Electrical transport measurements and (b) Raman spectra before and after oECM on the same contacted tube. The oECM was performed at +0.75 V versus Pt for 120 s in a solution of 10 mM 4-aminobenzylamine in ethanol. 0.1 M lithium perchlorate was used as a background electrolyte. (Reprinted with permission from [48].)

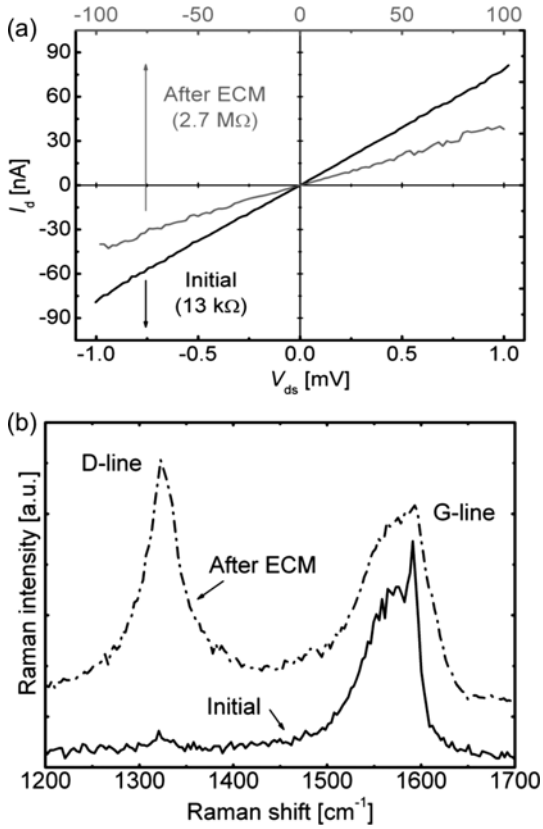

Figure 11 Reductive electrochemical modification (rECM) of individual contacted m-SWCNTs utilizing an aromatic diazonium salt. (a) Electrical transport measurements and (b) Raman spectra before and after rECM on the same contacted tube. The rECM was performed at −1.3 V versus Pt for 120 s in a solution of 10 mM 4-nitrobenzene diazonium tetrafluoroborate in *N*,*N*-dimethylformamide. 0.1 M lithium perchlorate was used as a background electrolyte. (Reprinted with permission from [48].)

lently [48]. While the former scheme is based upon the electrochemical generation of substituted phenyl radicals from aromatic diazonium salts, the latter involves the electrochemical oxidation of a substituted aromatic amine. Electrical transport and confocal Raman spectroscopic measurements on the same individual SWCNTs have been used to determine the respective bonding interaction between the formed polymer coating and nanotube. This is illustrated in Figs. 10 and 11, where the electrical resistance and Raman spectra of individual metallic nanotubes before and after the two kinds of modification are displayed. It is evident that the amine coupling brings in very few changes to the resistance and Raman spectra (Fig. 10), whereas the nanotube subjected to the diazonium coupling displays a strong increase in resistance (at least two orders of magnitude) and a D-line of significantly increased intensity (Fig. 11). Both features in the latter case signify the introduction of sp^3-bonded carbons into the nanotube framework, and hence confirm that the diazonium coupling results in the formation of covalent bonds.

3.4 Selective electrochemical functionalization

The major bottle-neck in the fabrication of FETs incorporating a SWCNT network as conducting channel is the fact that the synthetically available SWCNT material is composed of a mixture of both m- and s-SWCNTs. This hurdle has stimulated the development of methods for selective elimination of the m-SWCNTs. One intuitive method for this purpose involves the destruction of m-SWCNTs with high electrical currents. This has been realized through application of a large back-gate voltage in order to switch off the s-SWCNTs while a high drain bias is applied [49]. When performed under ambient conditions, high electric currents flow only through the m-SWCNTs which are hence burnt away through oxidation. Despite its increasing use, this method faces several difficulties, in particular when large, dense nanotube networks are to be modified, as the Joule heat generated in the m-SWCNTs increasingly affects adjacent s-SWCNTs. In addition, it requires the presence of a back gate that cannot be easily implemented on plastic substrates. One way around this problem is the transfer of the SWCNT network onto a different substrate

[50], which is however a tedious procedure. Furthermore, for higher tube densities substantial gate leakage can only be avoided if gate insulators of sufficiently large thickness are used, which in turn limits the electrostatic coupling of the back gate.

We have developed a selective electrochemical functionalization route to eliminate the m-SWCNTs in nanotube ensembles [51, 52]. The functionalization consists of the above described diazonium coupling. The covalent attachment of a high density of phenyl groups to the m-SWCNTs increases their electrical resistance by more than two orders of magnitude, whereby they are effectively eliminated from the electrical transport path. Selectivity of the electrochemical coupling to the m-SWCNTs has been achieved by two different methods. In the first approach [51], which has been originally developed for the back-gate configuration, advantage is taken of the hysteresis of the devices in order to switch the s-SWCNTs to the OFF state. After the completion of a gate cycle, these tubes remain switched off (at $V_G = 0$) for at least 15 minutes. During this time, the ECM is performed and mainly the m-SWCNTs are modified. Figure 12 compares typical transfer characteristics of devices containing between 10 and 20 SWCNTs before and after such electrochemical modification. With denser nanotube networks, however, problems arise due to a lower stability of the OFF state adjusted via the hysteresis.

In order to avoid this drawback, we have recently developed an alternative ECM scheme which does not require the presence of a back gate and is applicable also to denser networks [52]. This method relies upon the fact that a voltage V_{lG} applied to an Ag/AgCl liquid gate electrode has the same effect as applying a potential of $-V_{lG}$ to the working electrode (the contacted nanotube) versus Ag/AgCl [53]. Selective electrochemical coupling is then achieved by choosing a diazonium salt whose reduction peak potential lies in a voltage region where the s-SWCNT is in its OFF state. In order to verify this concept, we have calculated the reduction rates by using the Gerischer-Marcus model [32] analogous to Ref. [53] at a (9,0) m- and a (10,0) s-SWCNT for a range of diazonium salts with different reduction potentials [52]. Figure 13(a) presents the magnitudes of reduction rates at the two tubes for a diazonium salt whose reduction potential is chosen such that the s-SWCNT is gated to its OFF state. Correspondingly, Fig. 13(b) plots the relative reaction rate at the (9,0)- with respect to the (10,0)-SWCNT as a function of the liquid-gate voltage. It is apparent from the figure that by perform-

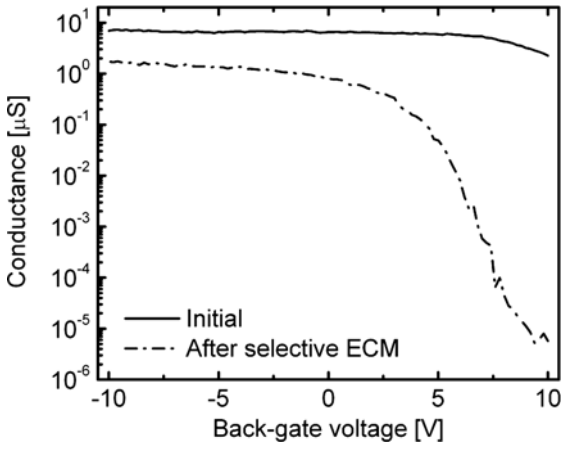

Figure 12 A nanotube FET obtained through back-gate assisted selective ECM of SWCNT bundles containing both m- and s-SWCNTs. The gate dependence of conductance initially shows metallic behaviour (solid line). After selective ECM, the conductance shows a variation of around 5 orders of magnitude (dash-dotted line) signifying that the m-SWCNTs have been eliminated. V_{ds} was 10 mV before ECM and 50 mV after ECM.

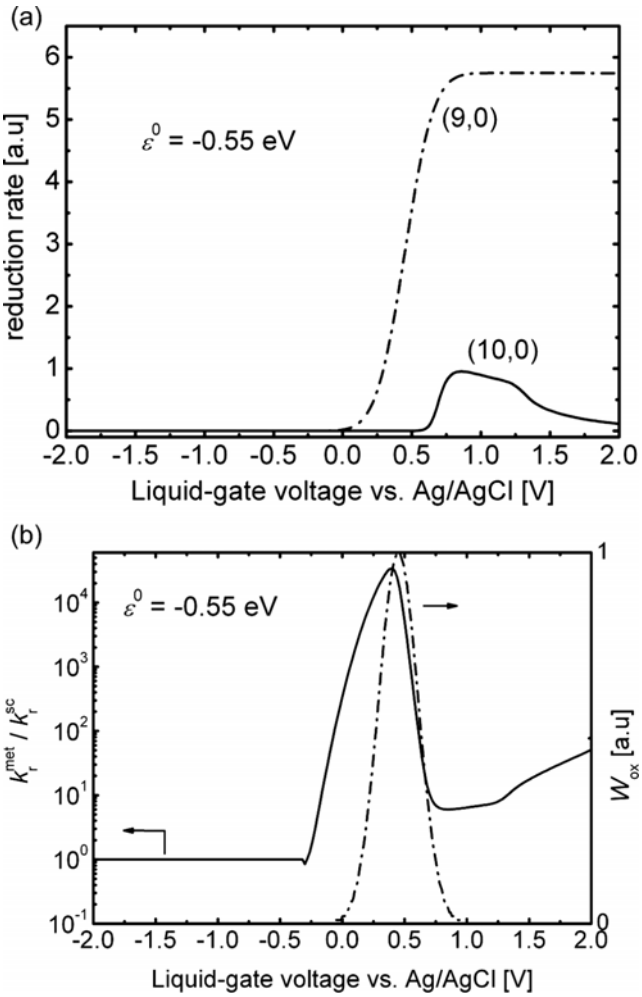

Figure 13 (a) Calculated magnitudes of electrochemical reduction rate (k_r) at a (9,0) m- and a (10,0) s-SWCNT with a coupling agent having a redox potential of $\varepsilon^0 = -0.55$ V. (b) Calculated relative reduction rate based on the k_r curves computed in (a). The dash-dotted line shows the calculated distribution of oxidized states (W_{ox}) for the redox couple with an ε^0 of -0.55 V. It is apparent that for a range of potentials around 0.3 V vs. Ag/AgCl, the reduction of the molecule at a (9,0) tube is around 4 orders of magnitude faster than at the (10,0) tube.

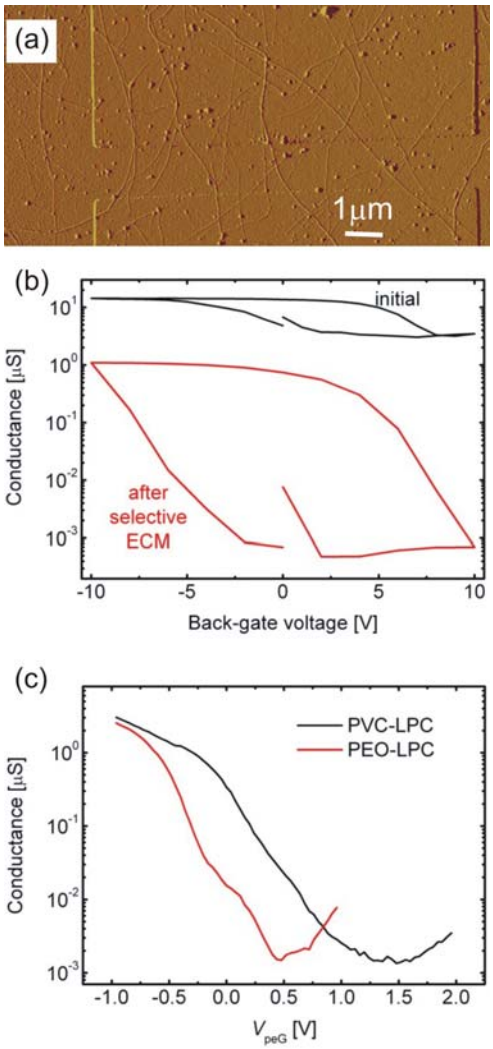

Figure 14 (online colour at: www.pss-a.com) FETs based on SWCNT networks: (a) Atomic Force Microscope (AFM) amplitude image of a network of tubes grown by chemical vapor deposition. (b) Gate dependence of conductance of such a network before and after selective ECM. V_{ds} is 10 mV before and 100 mV after ECM. (c) Variation of conductance of the same device after spotting two different solid polymer electrolytes and using an electrode in contact with the SPE as the gate ($V_{ds} = \pm 100$ mV). The composition of the SPE is identical to that in Fig. 9. V_{peG} is the voltage applied to the polymer electrolyte–gate.

ing the ECM at the denoted potential, the coupling to the m-SWCNT is expected to be more than five orders of magnitude faster than to the s-SWCNT. Thus, when this diazonium salt is combined with the suitable potential applied vs. Ag/AgCl, selective functionalization of dense networks of CVD-grown SWCNTs (see Fig. 14(a)) becomes possible. The transfer characteristics before and after selective ECM of this tube ensemble are depicted in Fig. 14(b), which reveal that the metallic tubes have been successfully eliminated and the device exhibits a good switching ratio of more than three orders of magnitude. It should be noted that the reproducibility of this method is low in case of SWCNT networks with a sizeable diameter distribution. The major complication arises from the presence of large-diameter metallic tubes that due to their small curvature have only a low chemical reactivity. This limitation may be overcome by a stricter control over the catalyst particle size and hence the nanotube diameter [13]. The nanotube networks modified in this manner can be subsequently coated with SPEs to obtain FETs operating at low voltages as shown in Fig. 14(c).

3.5 Chemical doping The implementation of complementary logic requires not only p-type but also n-type transistors. Chemical doping has proven to be a viable approach for converting p- into n-type SWCNT-FETs [54, 55], albeit the efficacy lacks significantly behind what would be needed for reliable technological application. Such conversion can be achieved with the aid of strong electron donors, among which the polymer polyethyleneimine (PEI) has turned out to yield most reproducible results [56, 57]. Figure 15(a) presents the transfer character-

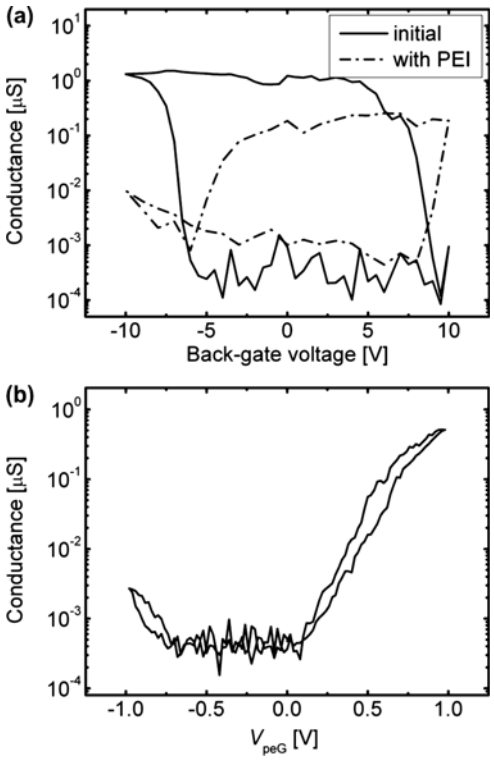

Figure 15 n-type doping of SWCNT-FETs. (a) Back gate dependence of conductance ($V_{ds} = \pm 100$ mV) for an s-SWCNT-FET before and after chemical modification with polyethyleneimine (PEI). A 33 wt% solution of PEI in methanol was spotted on the device and let to dry. The FET shows n-type characteristics after the modification, albeit still with a large hysteresis. (b) PEI can be used as a solid polymer electrolyte. The panel shows the variation of channel conductance as a function of the polymer electrolyte gate voltage (V_{peG}). An adjacent AuPd electrode on the substrate was used as the gate electrode ($V_{ds} = \pm 100$ mV).

istics of a SWCNT-FET before and after PEI doping. Due to its noticeable ionic conductivity, PEI serves at the same time as an SPE, and thus enables an adjacent electrode that is in touch with the PEI layer to act as a gate (see Fig. 15(b)). However, the life-time of PEI-coated SWCNT-FETs, in both the back gated and electrochemically gated configurations is very limited when the devices are stored under ambient, which is a consequence of the low air stability of PEI. In most cases, after more than 7 days the transistors show very high resistances (in the GΩ range) and loose their switching capability. Other donor compounds that have been studied for p- to n-type conversion of CNT-FETs are tetrathiafulvalene (TTF) [58], hydrazine [59], aminosilanes [60] and polyaniline [59]. However, like in the case of PEI, both the reproducibility of doping and the stability of the obtained n-type behavior are still posing a serious problem.

3.6 Sensors based on functionalized SWCNT-FETs The electric field effect in SWCNT-FETs offers the possibility to detect chemical species by exploiting charge transfer to the nanotube or changes in the tube's surface potential occurring upon molecular adsorption onto the nanotube channel. In this manner, a wide range of different (bio-)chemical sensors with impressively high sensitivities have been realized during the past few years [40, 41]. One example is the use of a liquid-gated s-SWCNT-FET to detect ammonia in solution at concentrations as low as 1 mM [29]. Adsorption of ammonia molecules onto the s-SWCNT leads to charge transfer and thereby shifts the threshold voltage of the liquid-gated nanotube transistor.

Along these lines, we have extended the electrochemical functionalization method to fabricate gas and chemical sensors based upon SWCNTs. For the aim of hydrogen sensing, SWCNT networks have been decorated with palladium nanoparticles via electroreduction of a Pd-containing salt [61]. Hydrogen is known to dissolve in Pd forming atomic hydrogen, with concomitant alteration of the work function of the Pd particles [62]. The resulting electron transfer onto the semiconducting tubes contained in the network triggers an increase of resistance of the Pd-modified nanotube network. The key advantage of the ECM method is the control over the Pd particle size and density, as well as the intimate coupling between particles and nanotube originating from their direct formation on the tube sidewalls. Toward the application of SWCNTs in liquid chemical sensors, we have developed a novel ECM strategy that can be applied to m-SWCNTs [63]. It comprises the covalent attachment of organic moieties bearing amino groups in a controlled density to individual metallic tubes. The resistance increase observed for the functionalized tubes upon increasing protonation of the appended basic groups has been assigned to an enhanced scattering strength for carriers in the nanotube. That this mechanism is dominant for the functionalized m-SWCNTs is confirmed by the low threshold shifts recently observed on pristine semiconducting nanotubes [39]. While the realization of such pH sensors served as a proof-of-principle, a similar mechanism may be exploited for the detection of other chemical species such as metal ions.

4 Device characterization of CNT-FETs Due to the significant distribution of diameter and chirality of the nanotubes in the raw material, it is important to characterize SWCNTs incorporated into an FET configuration individually. In this section, we discuss the important device parameters of CNT-FETs fabricated in the two gating configurations. Following this, we introduce a novel device characterization technique based upon local photocurrent detection, which enables the estimation of electronic band profiles of back-gated CNT-FETs.

4.1 Back-gated devices

4.1.1 Saturation In conventional MOSFETs, saturation is reached when the channel is pinched-off. It is an important device characteristic forming a key element of digital circuits [64]. In long-channel MOSFETs, saturation arises due to carrier-carrier interaction via Coulomb repulsion [65]. By contrast, the fact that SWCNT-FETs are unconventional SB-FETs brings in different mechanisms like velocity saturation [66]. In order for this mechanism to be effective, the carriers must experience negligible scattering by impurities or defects [67]. While this appears to be fulfilled in high-performance SWCNT-FETs [38, 43, 50], complete saturation is usually not observed in FETs fabricated on SiO_2 substrates [4, 16].

4.1.2 Transconductance Transconductance is a measure of how fast the transistor is able to switch while sweeping the gate voltage, and is related to the gain of the transistor. It is given by the ratio of the change in drain current to the change in gate voltage at a constant drain-source bias. In order to aid the comparison between different devices, a normalized transconductance g_m is computed per unit channel width. FETs based on single s-SWCNTs in the back-gated configuration with varying dielectrics generally exhibit g_m values in the range of 10 S/cm to 30 S/cm [37, 43]. However, with top-gated s-SWCNT-FETs higher g_m values have been reported. For example, a transconductance of 60 S/cm was observed for a top-gated single s-SWCNT-FETs with ZrO_2 as the gate dielectric [38]. Interestingly, the g_m values of transistors based on nanotube networks also fall in the same range of 10 S/cm to 30 S/cm. FETs obtained through selective elimination of m-SWCNTs in a low density network displayed g_m values close to 10 S/cm [51]. With highly ordered networks of high tube density, where the m-SWCNTs are eliminated via electrical breakdown, a transconductance of 30 S/cm has been reported [50].

4.1.3 Sub-threshold swing The sub-threshold swing is given by $S = \ln(10)\,[\mathrm{d}V_G/\mathrm{d}(\ln(I_d))] = (k_BT/e) \times \ln(10)\,(1/\alpha)$, where k_BT is the thermal energy at a temperature T (~24 meV for room temperature), e is the elec-

tronic charge, α is the gate coupling factor and V_G and I_d correspond to the gate voltage and drain current, respectively. The theoretical limit for S is 60 mV/decade at room temperature [31], corresponding to a maximum coupling efficiency of $\alpha = 1$. For most back-gated SWCNT-FETs (with oxide thickness ≥100 nm), a high value of S in the range of 100–2000 mV/decade is observed, corresponding to a low coupling efficiency α of between 0.6 and 0.03. The value of 60 mV/decade has been closely approached [38] or reached [43, 68] for single s-SWCNT-based FETs with optimized net device capacitance.

4.1.4 Mobility The mesoscopic size of CNTs renders it difficult to measure the intrinsic carrier mobility. Moreover, evaluation of the field-effect mobility from the transfer characteristics is hampered by the fact that the SWCNT-FETs normally behave as Schottky barrier transistors. Nonetheless, for the purpose of device comparison, it is reasonable to extract an effective field-effect mobility using $\mu = (dI_d/dV_G) \cdot L/(c_{net} V_{ds})$, where L is the channel length and c_{net} is the net capacitance per unit length. On this basis, impressive values as high as 100 000 cm^2/Vs have been reported for holes in a 325 μm long s-SWCNT at room temperature [3]. However, it should be kept in mind that, since the transconductance of SWCNT-FETs is often contact-limited, high-quality nanotubes of sufficient length can easily display extremely large effective field-effect mobilities. In comparison, SWCNT-FETs with channel lengths in the range of 100 nm to a few microns display lower values of a few 1000 cm^2/Vs. Similar values have been found for our FETs obtained via selective ECM. Compared to the mobility of holes, the electron mobility derived from the transfer characteristics of ambipolar-SWCNT-FETs is approximately one order of magnitude smaller. In the case of back-gated SWCNT networks, the ordering and alignment of the nanotubes across the source/drain electrodes play a crucial role in determining the carrier mobility. Disordered networks exhibit mobilities less than 50 cm^2/Vs, while with highly ordered tube arrays mobilities higher than 3000 cm^2/Vs have been reached [50].

4.2 Electrochemically gated devices Saturation in liquid-gated and polymer-electrolyte-gated devices is hardly observed, since the gate leakage increases exponentially for drain-source bias higher than 1 V. However, as the capacitances for the liquid-gated and polymer electrolyte-gated devices are very close to the quantum limit, the minimum possible sub-threshold swing can be reached. Typical values of sub-threshold swing obtained for liquid-gated and polymer electrolyte-gated devices are ~80 mV/decade, signifying a coupling efficiency close to 0.75 [31]. For single SWCNTs within PEO-based electrolytes, a transconductance of 5 S/cm is observed, corresponding to a field-effect mobility of ~2500 cm^2/Vs [33]. In case of SWCNT networks, the degree of ordering is a decisive factor, similar to the back-gated transistors. Highly-ordered networks [50] exhibit field-effect mobilities of the order of 3000 cm^2/Vs. However, a major disadvantage of the polymer electrolyte-gated transistors is that they cannot be operated at frequencies higher than 1 kHz [34].

4.3 Scanning photocurrent microscopy We have developed photoelectronic transport imaging [69] or scanning photocurrent microscopy (SPCM) [70] as an easy and fast method for determining band profiles of CNT-FETs with the aid of a confocal microscope. In this method, a diffraction-limited laser spot is used to illuminate the channel of CNT-FETs while simultaneously recording the local photoresponse. By choosing a channel length (>1.5 μm) much larger than the diameter of the diffraction-limited spot (~300 nm for λ_{exc} = 514.5 nm), it is possible to resolve the photocurrents originating from the middle of the channel from those at the contacts. In this manner, the

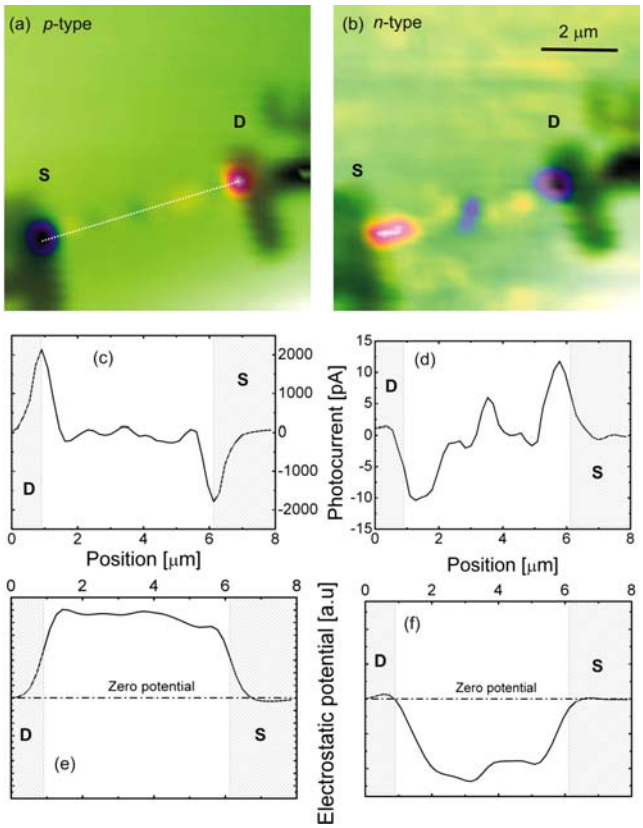

Figure 16 (online colour at: www.pss-a.com) Scanning photocurrent microscopy (SPCM) of an ambipolar s-SWCNT-FET with data recorded in the p-type (a, c, e) and n-type (b, d, f) regimes. (a, b) SPCM images showing the spatial variation of the photocurrent at zero drain–source bias. An optical image of the device is overlaid in order to identify the position of the contacts (black regions). (c, d) Line profiles of the photocurrent along the nanotube marked as a white dotted line in (a). The shaded regions indicate the position of the contacts. (e, f) Electrostatic potential maps obtained by integrating the corresponding line profiles in (c) and (d). The position of zero potential is marked by the dash-dotted line.

Schottky barriers at the contacts of a p-type SWCNT-FET at zero drain-source bias can be directly visualized, as shown in Fig. 16(a, c, e) [71]. When applied to ambipolar s-SWCNT-FETs, zero-bias photocurrent images acquired as a function of gate voltage reveal a reversal of the bending of the Schottky barriers upon transition from the p- to the n-type regime as shown in Fig. 16(b, d, f) [70]. On this basis, determination of the Schottky barrier height at the contacts can be accomplished in a straightforward manner. The obtained values for holes of the order of ~200 meV are in close correspondence with results of low-temperature conductivity measurements. Furthermore, qualitative electrostatic potential profiles are accessible through spatial integration of the photocurrents measured along the nanotube channel (Fig. 16(e, f)). Finally, photocurrent imaging has proven to be a versatile tool to identify tube defects [72] such as intratube junctions. The local electrical fields associated with such defects create additional signals along the nanotube (Fig. 16(b)).

5 Future perspectives One important advantage of the selective electrochemical functionalization approach is its direct applicability to nanotubes deposited on flexible (plastic) substrates. This would avoid the tedious transfer of the nanotubes between plastic and silicon substrates just for the sake of elimination of metallic tubes [50]. Another promising future perspective for ECM is the fabrication of gate insulators around the nanotubes, which could lead to the development of wrap-around gates offering optimal coupling of dielectric gates [73]. Moreover, the polymer electrolyte-based FETs could prove technologically relevant due to the ability to tune the threshold voltage just by varying the composition of the SPE. However, this task still requires a substantial improvement of the stability of the electrolyte material. One possible solution to this problem could be a hermetic sealing of the devices to avoid exposure to oxygen and ultraviolet (UV) light.

Further to this, the increasing activities in the field of biosensors based upon CNT-FETs could strongly benefit from the development of more elaborate (electro-)chemical functionalization methods, in particular with regard to achieving ultimate selectivity and biocompatibility [74]. Another stimulating impact may be on the elucidation of the exact mechanism by which SWCNT-FETs detect analytes in solution, specifically whether charge transfer or enhanced carrier scattering is the predominant effect of molecule adsorption [39, 75].

A major hurdle for the widespread application of SWCNTs in FETs is the current lack of synthesis or separation methods yielding exclusively semiconducting nanotubes, though significant progress has already been achieved in this direction. For instance, methods based on ion-exchange chromatography have shown promising results [76]. With the future advent of large-scale production methods of SWCNT with specified chirality and further advancements in the controlled growth of oriented SWCNT ensembles, combined with the help of the available chemical functionalization schemes, large-scale fabrication of high-performance thin film SWCNT-FETs should become feasible. First steps in this direction have very recently been reported [50, 76]. Important clues toward the minimization of defects in SWCNTs could be gained from microscopic techniques like scanning gate [77, 78] or scanning photocurrent microscopy [72, 79, 80]. The latter method offers the advantage of being applicable also to extended nanotube networks, and holds promise to provide valuable insights into the mechanism of inter-tube electrical transport.

6 Conclusion In summary, it is now well-established that semiconducting SWCNTs are close-to-ideal components of high-performance nanoscale FETs, albeit some of their intrinsic features posing serious challenges to the device fabrication. Foremost, the high sensitivity of s-SWCNTs against electric charges in their neighborhood renders them susceptible to minute changes in their environment. Chemical functionalization represents a valuable approach to improve the performance of SWCNT-FETs, with electrochemical methods being particularly useful due to their inherent capability to control the functionalization extent of the tubes, as well as to restrict the modification to the nanotube channel. One of the most exciting developments in CNT electrochemistry is the selective functionalization of metallic nanotubes contained within an ensemble, which provides for an effective route to FETs whose channel is comprised of a SWCNT network. Moreover, the emergence of novel powerful characterization techniques such as scanning photocurrent microscopy promises further elucidation of the operation mechanism of SWCNT-FETs.

Acknowledgements This work was supported by the Deutsche Forschungsgemeinschaft within the framework of the priority program SPP1121. We are grateful to F. Nan, M. Scolari, and A. Mews from the University of Siegen (Germany) for their continuous supply with CVD-grown SWCNTs and their close collaboration on confocal microscopy of individual nanotubes. We thank H. Klauk and U. Zschieschang for the help with the fabrication of nanotube transistors incorporating a SAM-based dielectric.

References

[1] G. Cuniberti, G. Fagas, and K. Richter (eds.), Introducing Molecular Electronics – Lecture Notes in Physics, Vol. 680 (Springer Verlag, Berlin–Heidelberg, 2005).
[2] Z. Yao, C. L. Kane, and C. Dekker, Phys. Rev. Lett. **84**, 2941 (2000).
[3] T. Durkop, S. A. Getty, E. Cobas and M. S. Fuhrer, Nano Lett. **4**, 35 (2004).
[4] S. J. Tans, M. H. Devoret, H. Dai, A. Thess, R. E. Smalley, L. J. Geerligs, and C. Dekker, Nature **386**, 474 (1998).
[5] A. Bachtold, P. Hadley, T. Nakanishi, and C. Dekker, Science **294**, 1317 (2001).
[6] J. B. Cui, R. Sordan, M. Burghard, and K. Kern, Appl. Phys. Lett. **81**, 3260 (2002).

[7] T. W. Ebbesen and P. M. Ajayan, Nature **358**, 220 (1992).
[8] T. Guo, P. Nikolaev, A. Thess, D. T. Colbert, and R. E. Smalley, Chem. Phys. Lett. **243**, 49 (1995).
[9] M. J. Bronikowski, P. A. Willis, D. T. Colbert, K. A. Smith, and R. E. Smalley, J. Vac. Sci. Technol. A **19**, 1800 (2001).
[10] J. Kong, A. M. Cassell, and H. J. Dai, Chem. Phys. Lett. **292**, 567 (1998).
[11] Y. Murakami, Y. Miyauchi, S. Chiashi, and S. Maruyama, Chem. Phys. Lett. **374**, 53 (2003).
[12] D. S. Bethune, C. H. Kiang, M. S. DeVries, G. Gorman, R. Savoy, and R. Beyers, Nature **363**, 605 (1993).
[13] Y. Li, W. Kim, Y. Zhang, M. Rolandi, D. Wang, and H. Dai, J. Phys. Chem. B **105**, 11424 (2001).
[14] R. Saito, G. Dresselhaus, and M. S. Dresselhaus, Physical Properties of Carbon Nanotubes (Imperial College Press, London, 1998).
[15] J. W. G. Wilder, L. C. Venema, A. G. Rinzler, R. E. Smalley, and C. Dekker, Nature **391**, 59 (1998).
[16] R. Martel, T. Schmidt, H. R. Shea, T. Hertel, and Ph. Avouris, Appl. Phys. Lett. **73**, 2447 (1998).
[17] S. Heinze, J. Tersoff, R. Martel, V. Derycke, J. Appenzeller and Ph. Avouris, Phys. Rev. Lett. **89**, 106801 (2002).
[18] W. Kim, A. Javey, R. Tu, J. Cao, Q. Wang, and H. Dai, Appl. Phys. Lett. **87**, 173101 (2005).
[19] V. Derycke, R. Martel, J. Appenzeller, and P. Avouris, Appl. Phys. Lett. **80**, 2773 (2002).
[20] J. Appenzeller, J. Knoch, V. Derycke, R. Martel, S. Wind, and Ph. Avouris, Phys. Rev. Lett. **89**, 126801 (2002).
[21] Y. F. Chen and M. S. Fuhrer, Nano Lett. **6**, 2158 (2006).
[22] R. Martel, V. Derycke, C. Lavoie, J. Appenzeller, K. K. Chan, J. Tersoff, and Ph. Avouris, Phys. Rev. Lett. **87**, 256805 (2001).
[23] A. Javey, J. Guo, Q. Wang, M. Lundstrom, and H. Dai, Nature **424**, 654 (2003).
[24] P. G. Collins, K. Bradley, M. Ishigami, and A. Zettl, Science **287**, 1801 (2000).
[25] F. Leonard and J. Tersoff, Phys. Rev. Lett. **84**, 4693 (2000).
[26] Z. Chen, J. Appenzeller, J. Knoch, Y. Lin, and P. Avouris, Nano Lett. **5**, 1497 (2005).
[27] R. Sordan, K. Balasubramanian, M. Burghard, and K. Kern, Appl. Phys. Lett. **88**, 053119 (2006).
[28] W. Kim, A. Javey, O. Vermesh, Q. Wang, Y. Li and H. Dai, Nano Lett. **3**, 193 (2003).
[29] K. Bradley, J. C. P. Gabriel, M. Briman, A. Star, and G. Gruner, Phys. Rev. Lett. **91**, 218301 (2003).
[30] M. Krueger, M. R. Buitelaar, T. Nussbaumer, C. Schoenenberger, and L. Forro, Appl. Phys. Lett. **78**, 1291 (2001).
[31] S. Rosenblatt, Y. Yaish, J. Park, J. Gore, V. Sazonova, and P. L. McEuen, Nano Lett. **2**, 869 (2002).
[32] A. J. Bard and L. R. Faulkner, Electrochemical Methods: Fundamentals and Applications (John Wiley and Sons, New York, 2001).
[33] C. Lu, Q. Fu, S. Huang, and J. Liu, Nano Lett. **4**, 623 (2004).
[34] T. Ozel, A. Gaur, J. A. Rogers, and M. Shim, Nano Lett. **5**, 905 (2005).
[35] J. Lee, M. J. Panzer, Y. He, T. P. Lodge, and C. D. Frisbie, J. Am. Chem. Soc. **129**, 4532 (2007).
[36] P. Avouris, Acc. Chem. Res. **35**, 1026 (2002).
[37] S. J. Wind, J. Appenzeller, R. Martel, V. Derycke, and P. Avouris, Appl. Phys. Lett. **80**, 3817 (2002).
[38] A. Javey, H. Kim, M. Brink, Q. Wang, A. Ural, J. Gu, P. McIntyre, P. L. McEuen, M. Lundstrom, and H. Dai, Nature Mater. **1**, 241 (2002).
[39] J. H. Back and M. Shim, J. Phys. Chem. B **110**, 23736 (2006).
[40] G. Gruner, Anal. Bioanal. Chem. **384**, 322 (2006).
[41] K. Balasubramanian and M. Burghard, Anal. Bioanal. Chem. **385**, 452 (2006).
[42] M. Burghard, Surf. Sci. Rep. **58**, 1 (2005).
[43] R. T. Weitz, U. Zschieschang, F. Effenberger, H. Klauk, M. Burghard, and K. Kern, Nano Lett. **7**, 22 (2007).
[44] S. Rajendran and T. Uma, J. Power Sources **88**, 282 (2000).
[45] V. S. Kolosnitsyn, G. P. Dukhanin, S. A. Dumler, and I. A. Novakov, Russ. J. Appl. Chem. **78**, 1 (2005).
[46] S. E. Kooi, U. Schlecht, M. Burghard, and K. Kern, Angew. Chem. Int. Ed. **41**, 1353 (2002).
[47] K. Balasubramanian and M. Burghard, Small **2**, 180 (2005).
[48] K. Balasubramanian, M. Friedrich, C. Jiang, Y. Fan, A. Mews, M. Burghard, and K. Kern, Adv. Mater. **15**, 1515 (2003).
[49] P. G. Collins, M. S. Arnold and P. Avouris, Science **292**, 706 (2001).
[50] S. J. Kang, C. Kocabas, T. Ozel, M. Shim, N. Pimparkar, M. A. Alam, S. V. Rotkin and J. A. Rogers, Nature Nanotechnol. **2**, 230 (2007).
[51] K. Balasubramanian, R. Sordan, M. Burghard, and K. Kern, Nano Lett. **4**, 827 (2004).
[52] K. Balasubramanian, M. Burghard, and K. Kern, submitted.
[53] I. Heller, J. Kong, K. A. Williams, C. Dekker and S. G. Lemay, J. Am. Chem. Soc. **128**, 7353 (2006).
[54] C. W. Zhou, J. Kong, E. Yenilmez, and H. Dai, Science **290**, 1552 (2000).
[55] P. Avouris and J. Chen, Mater. Today **9**, 26 (2006).
[56] M. Shim, A. Javey, N. W. S. Kam, and H. Dai, J. Am. Chem. Soc. **123**, 11512 (2001)
[57] G. P. Siddons, D. Merchin, J. H. Back, J. K. Jeong, and M. Shim, Nano Lett. **4**, 927 (2004).
[58] T. Takenobu, T. Takano, M. Shiraishi, Y. Murakami, M. Ata, H. Kataura, Y. Achiba, and Y. Iwasa, Nature Mater. **2**, 683 (2003).
[59] C. Klinke, J. Chen, A. Afzali, and P. Avouris, Nano Lett. **5**, 555 (2005).
[60] J. Kong and H. Dai, J. Phys. Chem. B **105**, 2890 (2001).
[61] U. Schlecht, K. Balasubramanian, M. Burghard, and K. Kern, Appl. Surf. Sci. **253**(20), 8394 (2007).
[62] I. Lundstroem, M. Armgarth, and L. G. Petersson, CRC Crit. Rev. Solid State Mater. Sci. **15**, 201 (1989).
[63] A. Maroto, K. Balasubramanian, M. Burghard, and K. Kern, Chem. Phys. Chem. **8**, 220 (2007).
[64] S. M. Sze, Physics of Semiconductor Devices (John Wiley and Sons, New York, 1981).
[65] W. Schockley, Proc. IRE **40**, 1365 (1952).
[66] Y. F. Chen and M. S. Fuhrer, phys. stat. sol. (b) **243**, 3403 (2006).
[67] T. Yamada, Appl. Phys. Lett. **76**, 628 (2000).
[68] Y. R. Lu, S. Bangsaruntip, X. Wang, L. Zhang, Y. Nishi and H. Dai, J. Am. Chem. Soc. **128**, 3518 (2006).
[69] K. Balasubramanian, M. Friedrich, Y. Fan, U. Wannek, A. Mews, M. Burghard, and K. Kern, Appl. Phys. Lett. **84**, 2400 (2004).

[70] E. J. H. Lee, K. Balasubramanian, J. Dorfmueller, Ralf Vogelgesang, Nan Fu, A. Mews, M. Burghard, and K. Kern, cond-mat arXiv:0705.3407v1 (2007).
[71] K. Balasubramanian and M. Burghard, Semicond. Sci. Technol. **21**, S22 (2006).
[72] K. Balasubramanian, M. Burghard, K. Kern, M. Scolari, and A. Mews, Nano Lett. **5**, 507 (2005).
[73] W. B. Choi, E. Bae, D. Kang, S. Chae, B. Cheong, J. Ko, E. Lee, and W. Park, Nanotechnology **15**, S512 (2004).
[74] B. L. Allen, P. D. Kichambare, and A. Star, Adv. Mater. **19**, 1439 (2007).
[75] D. S. Hecht, R. J. A. Ramirez, M. Briman, E. Artukovic, K. S. Chichak, J. F. Stoddart, and G. Gruener, Nano Lett. **6**, 2031 (2006).
[76] M. Zheng and E. D. Semke, J. Am. Chem. Soc. **129**, 6084 (2007).
[77] M. Bocrath, W. Liang, D. Bozovic, J. H. Hafner, C. M. Lieber, M. Tinkham, and H. Park, Science **291**, 283 (2001).
[78] M. Freitag, A. T. Johnson, S. V. Kalinin, and D. A. Bonnell, Phys. Rev. Lett. **89**, 216801 (2002).
[79] M. Freitag, J. C. Tsang, A. Bol, D. Yuan, J. Liu, and P. Avouris, Appl. Phys. Lett. **91**, 031101 (2007).
[80] Y. H. Ahn, W. Tsen, B. Kim, Y. W. Park, and J. Park, cond-mat arXiv:0707.3176 (2007).

